BIOCHEMISTRY
including biophysical chemistry & molecular biology
Article

Biochemistry **2010,** *49,* 6021–6032 6021
DOI: 10.1021/bi902231c

Role of Citrate and Phosphate Anions in the Mechanism of Iron(III) Sequestration by Ferric Binding Protein: Kinetic Studies of the Formation of the Holoprotein of Wild-Type FbpA and Its Engineered Mutants†

Katherine D. Weaver,[‡] Mario Gabričević,[‡,∥] Damon S. Anderson,[§,⊥] Pratima Adhikari,[§,@] Timothy A. Mietzner,[§] and Alvin L. Crumbliss*[,‡]

[‡]*Department of Chemistry, Duke University, Durham, North Carolina 27708, and* [§]*Department of Microbiology and Molecular Genetics, University of Pittsburgh School of Medicine, Pittsburgh, Pennsylvania 15206*
[∥]*Present address: Faculty of Pharmacy and Biochemistry, University of Zagreb, Zagreb, Croatia.*
[⊥]*Present address: Department of Pathology, Children's Hospital Boston, Boston, MA 02115.*
[@]*Present address: Dalton State College, Dalton, GA 30720.*

Received December 31, 2009; Revised Manuscript Received May 23, 2010

ABSTRACT: Ferric binding protein A (FbpA) plays a central role in the iron acquisition processes of pathogenic *Neisseria gonorrheae*, *Neisseria meningitidis*, and *Haemophilus influenzae*. FbpA functions as an iron shuttle within the periplasmic space of these Gram-negative human pathogens. Iron is picked up by FbpA at the periplasmic aspect of the outer membrane with concomitant acquisition of a synergistic anion. Here we report the kinetics and mechanisms involved with loading of iron(III) into iron-free FbpA using iron(III) citrate as an iron source in the presence of excess citrate or phosphate (physiologically available anions) at pH 6.5. In the presence of excess phosphate, iron(III) citrate loads into apo-FbpA in three kinetically distinguishable steps, while in the presence of excess citrate, only two steps are discernible. A stable intermediate containing iron(III) citrate-bound FbpA is observed in each case. The observation of an additional kinetic step and moderate increase in apparent rate constants suggests an active role for phosphate in the iron insertion process. To further elucidate a mechanism for iron loading, we report on the sequestration kinetics of iron(III) citrate in the presence of phosphate with binding site mutant apo-FbpAs, H9E, E57D, E57Q, Q58A, Y195F, and Y196H. Tyrosine mutations drastically alter the kinetics and hamper iron sequestration ability. H9E, E57D, and E57Q have near native iron sequestration behavior; however, iron binding rates are altered, enabling assignment of sequential side chain interactions. Additionally, this investigation elaborates on the function of FbpA as a carrier for iron chelates as well as "naked" or free iron as originally proposed.

Iron is one of the most abundant elements in the earth's crust. Much of the biosphere has incorporated this element as an essential mineral; that is, most life on this planet cannot exist without iron. Paradoxically, ferric iron (Fe^{3+}) is almost insoluble under normal physiological conditions and is capable of catalyzing the formation of reactive oxygen species, thus requiring seclusion from the aerobic, aqueous, and neutral pH of the cellular environment. Plants, higher animals, and other life forms have developed many specialized mechanisms that compete directly for iron within the environment. One such competition is exemplified by the struggle for iron between a human host and a bacterial pathogen. The role of iron as an essential cofactor in the metabolic pathways of both microorganisms and their hosts has shaped the relationship between host and pathogen. The host's defense mechanism is to exclude free iron as a nutritional resource through complexation with proteins (*1*). Pathogens counter this host defensive mechanism through exploitation of the host proteins as a nutritional resource and as a result use the host's control of iron to provide a soluble iron store.

Iron is a limiting growth factor for most microbes, and the efficient solubilization, transport, and storage of iron in pathogenic bacteria are indices of virulence (*2*). Gram-negative bacteria such as *Neisseria* and *Haemophilus* acquire iron from human iron transport proteins, lactoferrin and transferrin, and low-molecular weight iron chelators such as citric acid (*3*). Using receptors on their outer membranes, these bacteria dock the human proteins or iron chelators and induce release of their iron load. Once iron has passed from the host protein through the bacterial external membrane, it is shuttled across the periplasm to the inner cell membrane. To prevent hydrolysis and redox cycling, iron is transported across the periplasm via an Fe^{3+} specific binding protein named ferric binding protein (FbpA).[1] FbpA is a 34 kDa periplasmic binding protein which sequesters iron and serves as the auxiliary domain of the ABC (ATP-binding cassette) transporter FbpABC, which actively transports iron across the inner cellular membrane (*4*, *5*). The binding of iron to FbpA in the

†This study was supported by National Science Foundation Grants CHE 0418006, CHE 0809466, and DGE 0209592 (M.G.) to A.L.C. K. D.W. was supported in part by National Institutes of Health Biological Chemistry Training Grant GM08558. We thank the Fulbright Association for a fellowship to M.G.

*To whom correspondence should be addressed. Telephone: (919) 660-1540. Fax: (919) 660-1605. E-mail: Alvin.Crumbliss@duke.edu.

[1]Abbreviations: FbpA, ferric binding protein; Fe(Cit)′, distribution of iron(III) citrate complexes under the conditions given (see Experimental Procedures); WT, wild-type; CD, circular dichroism; LMCT, ligand-to-metal charge-transfer band.

Published on Web 05/24/2010

periplasm serves as a nodal point for the entry of iron into the cytoplasm since both iron salts (e.g., iron phosphate) and iron chelates (e.g., iron citrate) are transported by FbpA.

Neisseria are obligate human pathogens and as such are restricted to growth in biological fluids. Low-molecular weight ionic nutrients must pass through the periplasm, which lies between the porous outer membrane and the semipermeable cytoplasmic membrane. The anion composition of the periplasm is not well characterized but likely reflects the external host or cellular environment (*6*). In vivo, transferrin-bound iron is the major nutrient iron source for *Neisseria*. When transferrin-bound iron is not available, other sources of labile, chelated iron, if present in sufficient amounts, will sustain bacterial growth such as when the host defense system fails and the iron concentration is raised artificially (*7*−*9*).

In humans, the labile iron pool, commonly termed "non-transferrin-bound iron" (NTBI), is thought to consist of low-molecular weight, low-affinity chelators such as citrate, phosphate, or adenosine triphosphate (*10*). These small ferric ion complexes can cross the outer membrane of Gram-negative bacteria through nonspecific porins, and *Neisseria* have been reported to use citric acid as a heterologous siderophore (*11*−*13*). Phosphate and citrate concentrations in host extracellular fluids (1.0 and 0.1 mM, respectively) are expected to be normal constituents of the low-molecular weight component of the periplasm (*14*, *15*). However, the role of citrate and phosphate in the iron acquisition process of *Neisseria* has not been definitively determined.

It has been shown that FbpA has a high binding affinity for Fe^{3+} ($K_a = 10^{18}$ M^{-1}) in the presence of phosphate, and that concomitant exogenous anion binding is requisite (*16*). Many anions complement tight iron binding, including phosphate, arsenate, oxalate, nitrilotriacetate (NTA), sulfate, and citrate, and anion exchange is facile (*17*−*21*). The kinetics of both iron loading and iron release are paramount to the function of FbpA in shuttling iron across the periplasm between two membrane-bound receptor proteins. The geometry of the residues (two Tyr residues, one Glu, and one His) (*22*−*24*) used as donor groups for iron plays a significant role in FbpA's iron binding strength, and in the mechanism for sequestration and release. Here the mechanism of the iron loading process is probed using mutagenesis and rational design to provide different donor groups that are capable of satisfying the octahedral geometry requirements of iron. This study complements the previous mechanistic inferences derived from static crystals (*22*−*24*) and is directed toward two objectives: to establish the ability of the physiological chelator citrate to deliver iron to FbpA in the absence and presence of phosphate anion and to establish the kinetics and mechanism for the sequestration process at pH 6.5, the presumed pH of the periplasm. Although a role for phosphate was established previously (*25*), here we wish to explore whether this effect is also observed with the more biologically relevant citrate iron carrier, or if the mechanistic behavior of phosphate was dependent on NTA's presence as the iron carrier.

EXPERIMENTAL PROCEDURES

Materials. Citric acid monohydrate, NaOH, 2-(4-morpholino)-ethanesulfonic acid (MES), KCl, NaCl, and KOH were purchased from Fisher Scientific. Sodium phosphate dibasic (Na_2HPO_4), sodium perchlorate, and tris(hydroxymethyl)aminomethane (Tris base) were purchased from Sigma-Aldrich. Chelex-100 was purchased from Bio-Rad. All solutions were prepared using ultrapure 18 MΩ cm equivalent water (Hydropure) in acid-washed glassware.

Stock Solutions. (*i*) *Sodium Perchlorate*. A stock solution of sodium perchlorate, $NaClO_4$, was prepared from sodium perchlorate hydrate, $NaClO_4 \cdot xH_2O$, and filter sterilized though a 0.22 μm CA sterile filter system (Corning). Standardization of the $NaClO_4$ solution was performed by passing an aliquot through a strongly acidic cation exchange column packed with DOWEX 50W-X8, H^+, 20−50 mesh resin (J. T. Baker Chemical), and titrating the flow through with NaOH to a phenolphthalein end point.

(*ii*) *Ferric Perchlorate*. An acidic iron perchlorate $Fe(ClO_4)_3$ stock solution was prepared by dissolving $Fe(ClO_4)_3$ in 0.1 M $HClO_4$. The determination of the level of iron (0.104 M Fe^{3+}/0.1 M $HClO_4$) was performed by ultraviolet spectrophotometry (*26*).

(*iii*) *Ferric Citrate*. To avoid iron hydrolysis, working ferric citrate solutions were prepared by slow addition of an appropriate volume of an acidic $Fe(ClO_4)_3$ stock solution (0.104 M Fe^{3+}/0.1 M $HClO_4$) to a vigorously stirred solution of MES, citrate, and $NaClO_4$ for which the initial pH was adjusted to near neutral (approximately 6.7) by titration with 1 M NaOH before addition of acidic $Fe(ClO_4)_3$. In the neutral pH region with increasing citrate concentrations, iron complexation by citrate is favored over $Fe(OH)_n$ polymer formation, and the solutions remain a clear, golden color with no reddish-brown precipitate (*27*).

The ferric citrate equilibrium speciation was modeled using Hyperquad Simulation and Speciation (HySS) software for all concentrations in this study using previously reported affinity constants, keeping in mind the observation that iron is bound by FbpA at a 1:1 molar ratio (*28*). The speciation of iron(III) citrate depends on the citrate/iron(III) ratio, the concentrations of iron and citrate, the ionic strength of the solution, and the solution pH. Ferric citrate speciation was calculated using several models. Assuming that citric acid has three dissociable protons (H_3L), the model provided by Könisgberger generates a fairly constant source of the 1:1 and 1:2 species, $[Fe(Cit)OH]^-$ and $[Fe(Cit)_2OH]^{4-}$, respectively, at all concentrations used in this study (*29*, *30*). Using an alternate model proposed by Silva et al. using stability constants for citric acid with four dissociable protons (H_4L) at an ionic strength of 0.1 M, the prevalent iron(III) citrate species are $[Fe(Cit)_2]^{5-}$ and $[Fe(Cit)_2H]^{4-}$ over the concentration range used in our study (*29*−*31*). These models offer only an approximation of our system as input parameters are not available for our exact conditions (e.g., ionic strength and concentration). Given that iron(III) citrate speciation is indeed complex, and the addition of apo-FbpA will perturb the speciation further, throughout this paper the terminology Fe(Cit)′ will indicate that a mixed species distribution is present at the given iron(III) and citrate concentrations. The lack of variability of kinetic plots obtained over a range of Fe(Cit)′ and Cit concentrations and [Cit]:[Fe^{3+}] ratios suggests that within the range of concentrations used in our studies, minor variations in iron(III) citrate speciation do not influence our results or interpretations. The relevant concentrations in the stopped-flow cell after mixing were: 0.05−1 mM Fe^{3+} as Fe(Cit)′, ≈0.8−7.1 mM citrate, and 50 mM MES at an ionic strength of 0.15 ($NaClO_4$) and pH 6.5.

For reactions in the presence of excess phosphate, solutions were made similarly, except phosphate was present in solution prior to the addition of $Fe(ClO_4)_3$. Under these conditions, more than 99% of Fe^{3+} is present as the ternary complex Fe(Cit)-$(H_xPO_4)^{y-}$ (*32*). The relevant concentrations in the stopped-flow cell after mixing were 0.1−1 mM Fe^{3+} as Fe(Cit)$(H_xPO_4)^{y-}$, ≈0.1−1.1 mM citrate, 1.0−10 mM phosphate, and 50 mM MES at an ionic strength of 0.15 ($NaClO_4$) and pH 6.5.

The Fe(Cit)′ concentrations of the stock solutions (before mixing) ranged from 0.1 to 2 mM. Phosphate concentrations ranged from 2 to 20 mM. All Fe(Cit)′ solutions were allowed to stabilize overnight after preparation and were filter sterilized through a sterile SFCA 0.20 μm syringe filter (Corning) prior to use. Buffer pH adjustments were made using an Orion model 230A pH-meter.

Mutagenesis, Protein Expression, and Purification. The engineered iron binding mutants of FbpA were modeled on a computer using coordinates deposited into the Protein Data Bank. Substitutions for the iron binding side chains were added in standard geometries. A discussion of the replacements is included in the Supporting Information together with kinemages representing the mutants selected for expression and kinetic analysis (Figures S.9−S.14 of the Supporting Information). Recombinant FbpA cloned from *Neisseria gonorrheae* strain F62 was expressed in an *Escherichia coli* background with purification conducted as previously described (*4*). The Gene Editor System (Promega) was used to perform site-directed mutagenesis under the manufacturer's conditions using pSBGL as the template (*28*). Plasmid DNA was isolated from single putative mutants using standard miniprep techniques and was subjected to automated DNA sequencing using an ABI Prism 3100 sequencer operated by the Department of Microbiology and Molecular Genetics Shared Resources Facility, University of Pittsburgh. Oligonucleotide primers used for mutagenesis are listed in Table S.1 of the Supporting Information. Purified FbpA was bound to a carboxymethyl Sepharose column, and iron-loaded FbpA was converted to apo-FbpA on the column by addition of 10 volumes of 1 mM citrate in 0.1 M Tris base at pH 8.0. Apo-FbpA was eluted using a NaCl gradient in buffers rendered iron-free by exposure to Chelex-100. Fractions were collected in acid-washed glassware, extensively dialyzed against Chelex-100-treated 0.05 M MES with 0.2 M KCl, and concentrated using an Amicon centrifugal filter device (Millipore). Purified FbpA mutants were characterized using MALDI-TOF MS and circular dichroism (CD) analysis to monitor expected mass shifts and protein secondary structure (see Figures S.15−S.18 of the Supporting Information for MALDI-TOF MS and Figures S.19−S.24 of the Supporting Information for CD spectra). Aliquots were frozen and kept at liquid nitrogen vapor temperature until they were used for kinetic analysis.

In preparation for kinetic analysis, all protein solutions were dialyzed into Chelex-100-treated 0.05 M MES and 0.1 M NaCl prior to dialysis exchange into Chelex-100-treated kinetics buffer [0.05 M MES and 0.15 M $NaClO_4$ (pH 6.5)] to prevent precipitation between K^+ and ClO_4^-. Each dialysis treatment was allowed to proceed overnight in at least 1000:1 buffer:protein volume ratios.

Physical Measurements. Spectral studies were performed using a Varian Cary 100-Bio UV−vis spectrophotometer and Applied Photophysics stopped-flow SX.18 MV instrument equipped with a diode array spectrophotometer with an approximate range of 380−750 nm for rapid-scan measurements. Rapid-scan experiments provided evidence of the assignment of kinetic phases and conversion to the final product. Kinetic studies were performed using an Applied Photophysics SX.18 MV stopped-flow spectrophotometer and were monitored with both fluorescence and single-wavelength absorbance detection, with equivalent values of k_{obs} obtained for both detection modes. All kinetic data illustrated in the figures were obtained in fluorescence mode with excitation at 280 nm under pseudo-first-order (generally 10-fold excess) conditions of excess Fe(Cit)′ in 50 mM MES at an ionic strength of 0.15 ($NaClO_4$), pH 6.5, and 25 °C. The total fluorescence was monitored using a 305 nm cutoff filter. Each kinetic data point in the figures represents an average of two to seven replicate runs. Estimated errors are smaller than the data point size unless otherwise indicated. The dead time of the instrument is 1.4 ms as determined using the test reaction between 2,6-dichlorophenolindophenol and L-ascorbic acid (*33*). In all kinetic experiments probing citrate or phosphate dependencies, citrate or phosphate was present in both FbpA and Fe(Cit)′ solutions prior to mixing.

RESULTS

General Observations. Our objective in this work was to investigate the kinetics and mechanism of the delivery of iron from iron citrate to apo-FbpA in the absence and presence of phosphate. Time-resolved stopped-flow absorbance and fluorescence spectroscopy was used to detect the involvement of FbpA binding site side chains during sequestration of iron citrate. A generic form of the reaction in the absence and presence of phosphate is shown in eq 1

$$\text{apo-FbpA} + \text{FeL} \leftrightarrows \text{FeFbpA-L} \qquad (1)$$

where apo-FbpA represents the anion-bound form of the protein (apo-FbpA-Cit or apo-FbpA-PO_4), FeL represents the iron(III) chelate used to deliver Fe^{3+} [iron(III)−citrate or iron(III)−citrate−phosphate], and the product is the ternary iron(III)−protein−anion complex (FeFbpA-L). Results presented in subsequent sections demonstrate that iron sequestration proceeds via a kinetically distinguishable two-step process in the absence of phosphate and a three-step process in the presence of phosphate to produce FeFbpA-Cit as the kinetic product in both cases. Ultimately, in the presence of excess phosphate, anion exchange occurs, and FeFbpA-PO_4 is formed.

Kinetics of Insertion of Fe(Cit)′ into Apo-FbpA. The reaction of Fe(Cit)′ (see Experimental Procedures) with apo-FbpA in the presence of variable excess citrate concentrations was investigated as illustrated in eq 2.

$$\text{apo-FbpA-Cit} + \text{Fe(Cit)}' \rightarrow \text{FeFbpA-Cit} + \text{Cit} \qquad (2)$$

Under our experimental conditions, apo-FbpA exists as >94% FbpA-Cit (*19*). The spectral change that occurs during the Fe(III) sequestration reaction shown in eq 2 is illustrated in Figure 1. A quasi-equilibrium intermediate species is formed during the first process with a $t_{1/2}$ of 580 ms (0.1 mM Fe(Cit)′, 5 mM citrate, 70 μM FbpA, and pH 6.5), as indicated by the spectrum labeled Ic in Figure 1. In a second slower process, the intermediate species converts with a $t_{1/2}$ of 280 s to the spectrum labeled IIc in Figure 1. With a λ_{max} of 474 nm, this ligand-to-metal charge-transfer (LMCT) band is consistent with the formation of FeFbpA-Cit (*18*). The broad λ_{max} for the reaction product FeFbpA-Cit was confirmed independently using the Cary spectrophotometer in kinetic scanning mode, the final scan of which was compared directly with a spectrum of FeFbpA-Cit prepared separately. At longer times in the presence of a large excess of citrate, a third step (not shown) eventually results in the loss of the LMCT absorbance band as FeFbpA-Cit is deferrated to form iron citrate with a $t_{1/2}$ of 5 h. As components of the total iron citrate speciation denoted as Fe(Cit)′ in this work, nonreactive ferric citrate complexes must establish an equilibrium yielding a reactive FeCit species before interacting with FbpA in

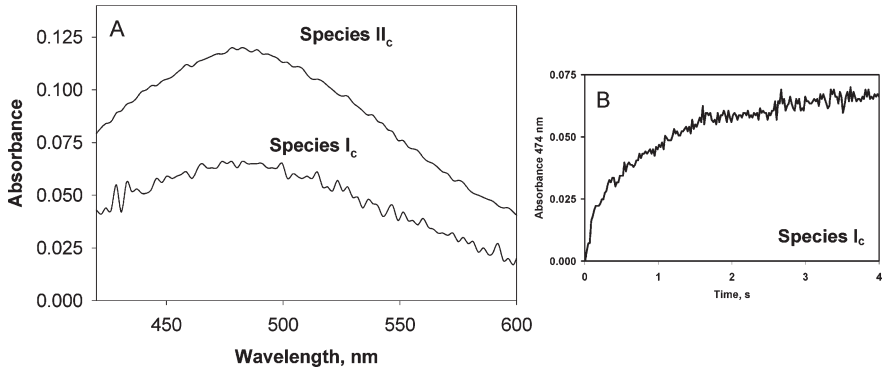

FIGURE 1: Absorbance spectra for the apo-FbpA-Cit + iron citrate reaction. (A) Absorbance spectra (λ_{max} = 474 nm) corresponding to quasi-equilibrium species Ic ($t_{1/2}$ = 0.58 s) and IIc ($t_{1/2}$ = 280 s) in Scheme 3. Conditions: 0.1 mM Fe(Cit)′, 5 mM citrate, 70 μM FbpA, 50 mM MES, pH 6.5, ionic strength of 0.15 ($NaClO_4$), and 25 °C. (B) Time domain profile for species Ic (time domain data for species IIc determined similarly).

a mechanism similar to that discussed by Bates for transferrin (*34*). On the basis of the disagreement of the complex speciation models, it is not apparent if the formation of a reactive 1:1 FeCit species like that reported by Bates is involved under these experimental conditions (*34*). However, the dependence on the citrate:Fe ratio is similar and does suggest that the formation of a reactive iron citrate species is involved in iron sequestration by FbpA. The rate of transfer of iron to FbpA and transferrin at low concentrations is dependent on ferric citrate, but at a high excess of citrate to iron, the reverse reaction becomes significant (*34*).

The kinetics of the steps involved in reaction 2 were investigated by stopped-flow absorbance and fluorescence spectroscopy as a function of Fe(III) and citrate concentrations. For transition metals, recognition of the metal center is communicated by fluorescence quenching where the quenched state indicates metal bound to the fluorophore (*35*, *36*). Although the 280 nm excitation wavelength generates both Trp and Tyr fluorescence, the use of both detection modes made it possible to determine whether the observed changes in fluorescence were due to (1) metal binding resulting in Tyr quenching or (2) fluorescence quenching due to changes in the environments of Trp residues. Both detection modes gave equivalent kinetic results where the fluorescence decline (Figure S.1 of the Supporting Information) corresponds to the Fe^{3+}-induced production of ionized tyrosine, the same species responsible for the increase in absorbance seen at a λ_{max} of 474 nm (Figure 1); i.e., the changes in fluorescence are comparable to those monitored in absorbance mode where only the tyrosines are reporting an increase in the magnitude of the LMCT band (*25*). The decrease in fluorescence (Figure S.1 of the Supporting Information) is ascribed to formation of the complex with the phenolates of the tyrosine residues during iron uptake in a process similar to that described for transferrins (*37*, *38*).

The observed pseudo-first-order rate constant for step Ic (k^{Ic}_{obs}) is independent of citrate and Fe(Cit)′ (Figure S.2 of the Supporting Information) concentrations. The plots agree within experimental error and level at a k^{Ic}_{obs} of ≈1.3(2) s^{-1}. We assume that this process is associated with a change in the conformation of the protein possibly induced by iron interaction at the N-terminal domain accompanied by proton loss as observed for transferrins (*37*, *38*). The second slower step (step IIc) continues to the completion of the reaction to form FeFbpA-Cit. The observed pseudo-first-order rate constant of the second step (k^{IIc}_{obs}) is not dependent on citrate concentration (Figure S.3 of the Supporting Information) but shows saturation behavior with respect to Fe(Cit)′ (Figure 2).

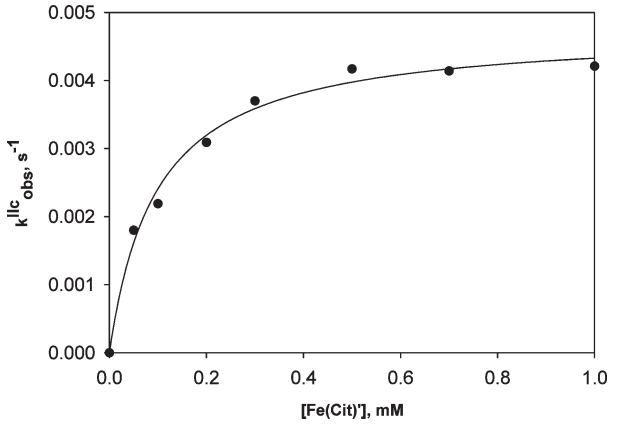

FIGURE 2: k_{obs} vs Fe(Cit)′ concentration for step IIc [FbpA-Cit + Fe(Cit)′]. All solutions were in 50 mM MES at an ionic strength of 0.15 ($NaClO_4$), pH 6.5, and 25 °C. Fluorescence mode conditions (after mixing): 5 mM citrate and 7 μM FbpA. The solid line represents a fit of eq 8 to the data. Estimated errors are smaller than the data point size.

Scheme 1

Step Ic

$$\text{FbpA} + \text{Cit} \leftrightarrows \text{FbpA-Cit} \quad (3)$$

$$Fe^{3+}_{aq} + \text{Citrate} \leftrightarrows \text{Fe(Cit)}' \quad (4)$$

$$\text{FbpA-Cit} + \text{Fe(Cit)}' \leftrightarrows \text{Fe(Cit)FbpA-Cit*} \qquad K_5,\ k_5 \quad (5)$$

Step IIc

$$\text{Fe(Cit)FbpA-Cit*} \rightarrow \text{FeFbpA-Cit} + \text{Cit} \qquad k_6 \quad (6)$$

Our proposed working model for the overall process in reaction 2 is illustrated in Scheme 1. We propose that step Ic in which 50% of the fluorescence is quenched is composed of three processes where FbpA and Fe^{3+}_{aq} are in equilibrium with citrate (reactions 3 and 4) as pre-equilibria to apo-FbpA-Cit reacting with Fe(Cit)′ (reaction 5). [See Experimental Procedures for a discussion of Fe(Cit) speciation as a function of the Fe^{3+}:citrate ratio.] In reaction 5, the asterisk denotes an intermediate state in which Fe(Cit)′ may be fully or partially complexed in the secondary coordination sphere by the FbpA binding site. Step II_C in which the other 50% of the fluorescence quenching occurs may be interpreted to involve the reorganization of Fe(Cit)-FbpA-Cit* to form a stable FeFbpA-Cit complex, where either the chelating citrate or a citrate pre-equilibrated with apo-FbpA is released from the binding site upon protein closure (reaction 6).

Table 1: Comparative Kinetic Data for Insertion of Fe(Cit)′ and Fe(NTA) into FbpA in the Absence of Phosphate

reaction	parameter	X = citrate[a]	X = NTA[b]
FeX + apo-FbpA-X ⇆ (FeX)FbpA-X*	$t_{1/2}$[c]	0.58(9) s	1.0(1) s
	k_5	1.3(2) s^{-1}[d]	2.6(1) × 10^3 M^{-1} s^{-1}
	K_5	1.0(2) × 10^4 M^{-1}[e]	1.1(1) × 10^4 M^{-1}
(FeX)FbpA-X* → FeFbpA-X	k_6	4.8(2) × 10^{-3} s^{-1}[e]	2.2(1) × 10^{-2} s^{-1}

[a]This work. All solutions in 50 mM MES at an ionic strength of 0.15 ($NaClO_4$), pH 6.5, and 25 °C. The error in the final digit is in parentheses. [b]Data from ref *25*. All solutions in 50 mM MES at an ionic strength of 0.15 ($NaClO_4$), pH 6.5, and 25 °C. The error of the final digit is in parentheses. [c]For step I, the Fe(Cit)′ reaction does not exhibit an Fe(Cit)′ concentration dependence, while the Fe(NTA) reaction is first-order with respect to Fe(NTA) concentration. For the sake of comparison, the half-life ($t_{1/2}$) for the formation of the intermediate (FeX)FbpA-X* (X = NTA or Cit) was determined under identical conditions: 0.4 mM Fe(Cit)′, 0.4 mM Fe(NTA), 7−8 μM FbpA, 50 mM MES, ionic strength of 0.15 ($NaClO_4$), pH 6.5, and 25 °C. [d]The error in the final digit is in parentheses and reports the reproducibility of the series of experiments whose results are given in Figure S.2 of the Supporting Information. The value reported is an average of the rate constants from Figure S.2: citrate dependency, 1.1(1), and Fe(Cit)′ dependency, 1.5(1), which are similar and thus are both considered representative of the kinetic process defined as step Ic. [e]Value obtained from a fit of eq 8 to data in Figure 2.

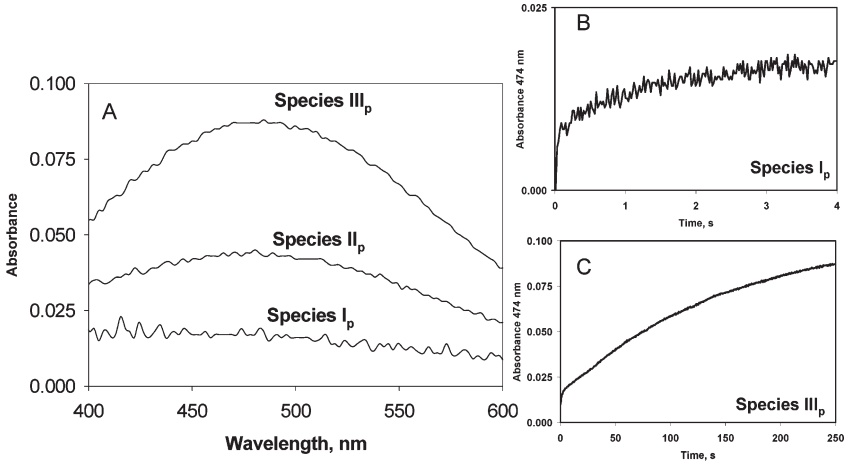

FIGURE 3: Absorbance spectra for the apo-FbpA-PO_4 + Fe(Cit)(PO_4) reaction. (A) Absorbance spectra (λ_{max} = 474 nm) corresponding to quasi-equilibrium species Ip ($t_{1/2}$ = 0.11 s), IIp ($t_{1/2}$ = 1.7 s), and IIIp ($t_{1/2}$ = 50 s) in Scheme 4. Conditions: 0.1 mM Fe(Cit)′, 50 μM FbpA, 5 mM $H_xPO_4^{y-}$, 50 mM MES, pH 6.5, ionic strength of 0.15 ($NaClO_4$), and 25 °C. (B) Time domain profile for species Ip. (C) Time domain profile for species IIIp. Time domain data for species IIp determined similarly.

This is consistent with the observed λ_{max} and absorptivity (Figure 1).

Step Ic corresponds to reactions 3−5, with reaction 5 being rate-limiting and reactions 3 and 4 being rapid pre-equilibria. Step IIc corresponds to reactions 3−6, where reactions 3−5 are pre-equilibria and reaction 6 is rate-limiting. Under pseudo-first-order conditions [where the Fe(Cit)′ concentration is much greater than the FbpA concentration], the experimentally observed rate for the overall process, including steps Ic and IIc, is defined in eq 7.

$$\text{rate}_{obs} = k_{obs}^{IIc}[\text{FbpA}]_{total} \quad (7)$$

From the overall rate expression in eq 7, and considering reaction 5 as a pre-equilibrium step, k_{obs}^{IIc} is defined as in eq 8.

$$k_{obs}^{IIc} = \frac{k_6 K_5 [\text{Fe(Cit)}']_t}{1 + K_5 [\text{Fe(Cit)}']_t} \quad (8)$$

A fit of the data to eq 8 is shown in Figure 2, and the following parameters were obtained: K_5 = 1.0(2) × 10^4 M^{-1}, and k_6 = 4.8(2) × 10^{-3} s^{-1} (Table 1, column 3). Inclusion of a term for the back reaction did not result in convergence of the parameters. According to the data presented, we conclude that excess citrate has no influence on the insertion of Fe(Cit)′ into apo-FbpA.

Kinetics of Insertion of Fe(Cit)′ into Apo-FbpA in the Presence of Phosphate. The reaction of Fe(Cit)′ with apo-FbpA in the presence of excess phosphate is illustrated in eq 9.

$$\text{FbpA-PO}_4 + \text{Fe(Cit)(PO}_4) \rightarrow \text{FeFbpA-Cit} + \text{PO}_4 \rightarrow \text{FeFbpA-PO}_4 + \text{Cit} \quad (9)$$

Depending on conditions and in the absence of exogenous citrate, more than 35% of apo-FbpA is complexed with phosphate at the anion binding site (FbpA-PO_4) prior to being mixed with Fe(Cit)′, which in the presence of phosphate yields Fe(Cit)-(PO_4) (*19*). The spectral change that occurs during the Fe(III) exchange reaction in eq 9 is shown in Figure 3. As opposed to reaction 2 in the absence of exogenous phosphate, two quasi-equilibrium intermediate species (labeled Ip and IIp in Figure 3) are formed with $t_{1/2}$ values of 110 ms and 1.7 s (at 0.1 mM Fe(Cit)′, 5 mM phosphate, 50 μM FbpA, and pH 6.5). In the second process, the intermediate species indicated by spectrum IIp is converted with a $t_{1/2}$ of 50 s to the spectrum labeled IIIp in Figure 3 (λ_{max} = 474 nm). This is consistent with the formation of FeFbpA-Cit (*18*). Eventually ($t_{1/2}$ = 20 h), the spectrum indicating FeFbpA-Cit formation shifts to a λ_{max} of 481 nm (data not shown), suggesting that citrate anion exchange occurs to form FeFbpA-PO_4 (*18*). An active role for phosphate in the Fe(III) sequestration process may be inferred from the fact that the Fe(Cit)′ sequestration reaction occurs more rapidly in the presence of phosphate and with the detection of an additional kinetic intermediate.

The relative amplitudes of the fluorescence mode kinetic traces for insertion of iron into FbpA from Fe(Cit)′ in the presence of phosphate are ~10, ~45, and ~45% for the first, second, and third steps, respectively. The working model for the overall process described in reaction 9 is illustrated in Scheme 2, where Step Ip corresponds to reactions 10−12, step IIp to reactions 10−13, and step IIIp to reaction 14.

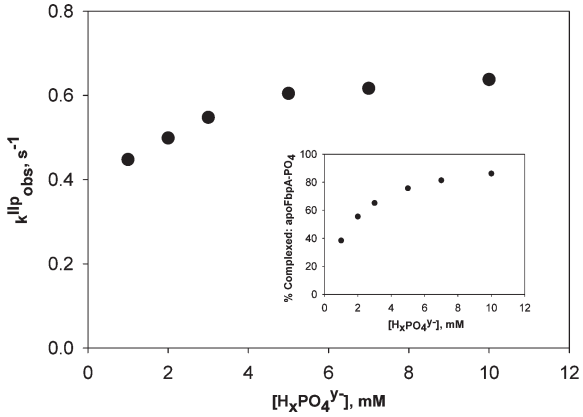

FIGURE 4: k_{obs} vs $H_xPO_4^{y-}$ concentration for step IIp [FbpA-PO_4 + Fe(Cit)(PO_4)]. All solutions in 50 mM MES at an ionic strength of 0.15 ($NaClO_4$), pH 6.5, and 25 °C. Fluorescence mode conditions (after mixing): 0.1 mM Fe(Cit)′ and 7 μM FbpA. Estimated errors are smaller than the data point size unless otherwise indicated. The inset is a plot of the percent formation of apo-FbpA-PO_4 as a function of phosphate concentration (eq 10) (*19*).

Scheme 2

Step Ip

$$FbpA + (H_xPO_4)^{y-} \leftrightarrows FbpA\text{-}PO_4 \qquad K_{10} \qquad (10)$$

$$Fe(Cit) + (H_xPO_4)^{y-} \leftrightarrows Fe(Cit)(H_xPO_4)^{y-} \qquad K_{11} \qquad (11)$$

$$FbpA\text{-}PO_4 + Fe(Cit)(H_xPO_4)^{y-} \leftrightarrows Fe(Cit)FbpA\text{-}PO_4{*} + (H_xPO_4)^{y-} \qquad K_{12} \qquad (12)$$

Step IIp

$$Fe(Cit)FbpA\text{-}PO_4{*} \underset{k_{13}}{\leftrightarrows} Fe(Cit)FbpA\text{-}PO_4{**} \qquad K_{13} \qquad (13)$$

Step IIIp

$$Fe(Cit)FbpA\text{-}PO_4{**} \leftrightarrows FeFbpA\text{-}Cit + (H_xPO_4)^{y-} \qquad (14)$$

In step Ip, no dependence on phosphate (Figure S.4 of the Supporting Information) or Fe(Cit)′ (Figure S.5 of the Supporting Information) concentration was observed. This suggests that the rate-determining step represented by a k^{Ip}_{obs} of 6 s^{-1} is likely due to a change in the conformation of the protein active site.

We observe saturation dependence on phosphate concentration (Figure 4) and no dependence on Fe(Cit)′ concentration (Figure S.6 of the Supporting Information) for the pseudo-first-order rate constant associated with step IIp. The rate-determining process in step IIp is illustrated in reaction 13. Reactions 10−12 from step Ip may be considered as pre-equilibria for reaction 13. The phosphate concentration dependence of the rate in Figure 4 may be attributed to the relative shift in equilibrium reaction 10 with an increase in phosphate concentration. This assertion is supported by a plot of the percent total protein complexed as apo-FbpA-PO_4 as a function of $H_xPO_4^{y-}$ concentration (Figure 4, inset) (*19*).

In step IIIp, no dependence on phosphate (Figure S.7 of the Supporting Information) or Fe(Cit)′ (Figure S.8 of the Supporting Information) concentration was observed, suggesting that the quasi-equilibrium in reaction 13 lies far to the right. We interpret this as an indication of another change in the conformation of the protein once the binding site is loaded with iron, also similar to the mechanism seen for lactoferrin (*37*). Leveling of k^{IIIp}_{obs} to form FeFbpA-Cit is at 1.5 × 10^{-2} s^{-1} (Figure S.7 of the Supporting Information) which is approximately 1 order of magnitude faster than without phosphate (Figure S.3 of the Supporting Information; see also Table 2, row 3, columns 2 and 4).

Comparison of Kinetics of Iron Transfer as a Function of Citrate and Phosphate Concentrations. For comparative analysis, in Table 2, we define a phenomenologically "apparent" first-order rate constant [k^{app} (s^{-1})] for each step in each system (with and without phosphate) under a fixed set of conditions for the Fe insertion reactions 2 and 9: 7 μM FbpA, 5 mM PO_4 or Cit, 1.0 mM Fe(Cit)′, pH 6.5, 50 mM MES, and ionic strength of 0.15 ($NaClO_4$). For the Fe^{3+} insertion process, we observe that substituting PO_4^{3-} for excess citrate and Fe(Cit)(PO_4) for Fe(Cit)′ results in a change from a two-step to a three-step resolvable system (Table 2).

Considering the relative percent fluorescence quenching observed for each of the steps, we tentatively conclude that there is an initial step in the presence of phosphate that is resolvable,

Table 2: Calculated Apparent Rate Constants for Insertion of Fe(Cit)′ and Fe(NTA) into Apo-FbpA in the Absence and Presence of Phosphate

	Fe(Cit)′		Fe(Cit)(PO_4)		Fe(NTA)		Fe(NTA)(PO_4)	
row	parameter value (s^{-1})[a]	%[e]	parameter value (s^{-1})[f]	%[e]	parameter value (s^{-1})[j]	%[e]	parameter value (s^{-1})[m]	%[e]
1	N/A[b]	N/A[b]	step Ip k_I^{app} = 6.0[g]	10	N/A[b]	N/A[b]	step I k_I^{app} = 80[n]	10
2	step Ic k_I^{app} = 1.3[c]	50	step IIp k_{II}^{app} = 0.6[h]	45	step I k_I^{app} = 2.8[k]	50	step II k_{II}^{app} = 0.7[o]	45
3	step IIc k_{II}^{app} = 0.0020[d]	50	step IIIp k_{III}^{app} = 0.015[i]	45	step II k_{II}^{app} = 0.022[l]	50	step III k_{III}^{app} = 0.0093[p]	45

[a]Apparent first-order rate constant for step Ic (k_I^{app}) and step IIc (k_{II}^{app}) calculated under the following conditions: 7 μM FbpA, 0 mM PO_4, 5 mM Cit, 1.0 mM Fe(Cit)′, 50 mM MES, ionic strength of 0.15 ($NaClO_4$), pH 6.5, and 25 °C. [b]Not observed. [c]This work. See Figure S.2 of the Supporting Information. [d]This work. See Figure 2. [e]Percent of total fluorescence quenching observed for this step. [f]Apparent first-order rate constant for step Ip (k_I^{app}), step IIp (k_{II}^{app}), and step IIIp (k_{III}^{app}) calculated under the following conditions: 7 μM FbpA, 5 mM PO_4, 0 mM Cit, 1.0 mM Fe(Cit)′, 50 mM MES, ionic strength of 0.15 ($NaClO_4$), pH 6.5, and 25 °C. [g]This work. See Figure S.5 of the Supporting Information. [h]This work. See Figure S.6 of the Supporting Information. [i]This work. See Figure S.8 of the Supporting Information. [j]Apparent first-order rate constant for step I (k_I^{app}) and step II (k_{II}^{app}) calculated under the following conditions: 8 μM FbpA, 0 mM PO_4, 1.0 mM Fe(NTA), 50 mM MES, ionic strength of 0.15 ($NaClO_4$), pH 6.5, and 25 °C. [k]From ref *25*. Value calculated by extrapolating data in Figure 6 to 1.0 mM Fe(NTA). [l]From ref *25* (Figure 6). [m]Apparent first-order rate constant for step I (k_I^{app}), step II (k_{II}^{app}), and step III (k_{III}^{app}) calculated under the following conditions: 7 μM FbpA, 5 mM PO_4, 1.0 mM Fe(NTA), 50 mM MES, ionic strength of 0.15 ($NaClO_4$), pH 6.5, and 25 °C. [n]From ref *25* (Figure 3). [o]From ref *25*. Extrapolated from data in Figure 4A. [p]From ref *25*. Calculated from data in Figure 5 and eq 12.

accounts for 10% of the observed fluorescence quenching (step Ip), and cannot be resolved in the absence of phosphate. The lack of this step in the absence of phosphate may have several origins, but it is likely that citrate may not preorganize the Tyr residues in the FbpA binding site to the same extent that PO_4^{3-} does. Also, citrate as a synergistic anion in the cleft of apo-FbpA is more sterically demanding than phosphate. The interaction of Fe(Cit)′ with a partially occupied apo-FbpA would place the approaching iron farther from the phenolic Tyrs during the initial step. This could cause less efficient quenching and result in the presence of iron not being reported. Also, there may be two initial steps in the citrate system, but both may be of the same magnitude and overlap enough that their half-life cannot be resolved. As a result, what is defined as step Ic for the citrate system may actually be a blending of two nonresolvable rate constants, while the presence of PO_4^{3-} enables resolution by increasing the rate of the early process.

The process represented by step IIp (45% fluorescence quench) may be compared with step Ic (50% fluorescence quench) and that represented by step IIIp (45% fluorescence quench) with step IIc (50% fluorescence quench) (see rows 2 and 3 of Table 2). k_I^{app} for step Ic and k_{II}^{app} for step IIp are comparable in value (Table 2, row 2, columns 2 and 4), and we observe an increase of approximately 1 order of magnitude for the last step (steps IIc and IIIp) in the presence of PO_4^{3-} to produce FeFbpA-Cit in both cases (cf. k_{II}^{app} and k_{III}^{app} in Table 2, row 3, columns 2 and 4). These comparative data suggest that PO_4^{3-} plays a role in the stepwise Fe^{3+} insertion process.

Kinetics of Insertion of Fe(Cit)′ into Engineered Apo-FbpA Mutants in the Presence of Phosphate. Kinetic experiments with protein point mutations were conducted to elucidate the involvement of specific binding site side chains in the Fe^{3+} sequestration process. A description of in silico experiments designed to evaluate the rational design of iron binding mutants of FbpA based on clashes and energetics is found in the Supporting Information. Mutations were chosen that did not incorporate significant changes to the conformation of neighboring side chains and that would test the kinetic properties of FbpA relevant to iron sequestration. The mutations were chosen to minimize the effects on the ability of the remaining residues to form coordinate covalent bonds to Fe^{3+} while providing alternate Fe^{3+} Lewis base ligands or removal thereof.

The point mutations utilized may be divided into two groups, those in the N-terminal domain (E57D, E57Q, H9E, and Q58A) and those in the C-terminal domain (Y195F and Y196H). Except for the tyrosine mutants, the overall amplitudes and shapes of the fluorescence mode kinetic traces for each of the mutants (E57D, E57Q, H9E, and Q58A) are similar to those of the wild type and suggest a similar iron binding motif (data not shown). The effects of protein point mutations on Fe^{3+} sequestration kinetics can be readily seen through a comparison of the ratio R of the rate constants for the corresponding steps ($R = k_{mutant}/k_{wt}$) and fluorescence quenching amplitudes for the wild-type (WT) protein. The reaction conditions used for comparison of the reaction of Fe(Cit)′ with apo-FbpA in the presence of excess phosphate (eq 9) and the ratios of first-order rate constants for the three steps, k_{obs}^{Ip}, k_{obs}^{IIp}, and k_{obs}^{IIIp}, are shown in Figure 5.

The E57D mutant on the N-terminal domain offers the same hard oxygen donor group but is not expected be at an optimized distance relative to WT for coordination to the Fe^{3+} center. Figure 5 illustrates the effect of the E57D mutant on k_{obs}^{Ip}, k_{obs}^{IIp}, and k_{obs}^{IIIp} data collected at both variable phosphate and Fe(Cit)′ concentrations in the presence of excess phosphate. The strongest influence is on k_{obs}^{Ip}, where in both cases R is approximately 0.5. This significant deviation from an R value of 1 observed for step Ip suggests the direct involvement of Glu57 early in the FeL binding process (eq 9).

N-Terminal domain effects were tested further by substitution of Glu57 with Gln, providing a polar, uncharged amide oxygen in a side chain of equivalent length and volume. Here the results are less dramatic with no change in the variable iron concentration R values for E57Q (Figure 5), but R is less than 1 with respect to variable phosphate concentration data for step Ip (k_{obs}^{Ip}) [R = 0.65 (Figure 5)]. This is consistent with the results for the E57D mutant, further confirming the direct involvement of Glu57 early in the FeL sequestration process.

The third N-terminal domain mutation, H9E, produces the most dramatic effect on step Ip ($R \sim 0.35$) for both Fe(Cit)′ and phosphate variable concentration data (Figure 5), consistent with initial sequestration events occurring in the N-terminal domain sites E57 and H9.

Although not directly involved in Fe^{3+} sequestration, the Q58A mutation tested the effects of synergistic anion hydrogen bonding on iron sequestration kinetics (*23*). Because of the limited expression levels and purification yields for Q58A, only data at the highest iron concentration were collected [10 mM Fe(Cit)′ after mixing]. Although Q58 is not directly involved in Fe^{3+} coordination, early stages (k_{obs}^{Ip} and k_{obs}^{IIp}) produced an R value of approximately 1.5 (Figure 5), suggesting more open access to the Fe^{3+} binding site with this mutation.

A limited number of mutants were expressed to explore a maximum number of effects, so only two Tyr mutants were examined: (1) Y195F which results in a loss of iron coordination from one residue and (2) Y196H which provides an alternate Lewis base for coordination [hard (O) vs borderline (N) Lewis base]. Very limited expression levels and yields were found for Y195F and Y196H, and as a result, only data at the highest iron concentration were collected [10 mM Fe(Cit)′ after mixing]. The shapes of the time domain fluorescence kinetic traces for both Tyr mutants were drastically altered from that of the wild type (data not shown). R values for Y195F and Y196H are significantly enhanced for step Ip [$R > 3$ (Figure 5)], suggesting that changes in exogenous anion H-bonding capability may produce a more openly accessible Fe^{3+} binding site in the early stages of sequestration. Step IIp for Y196H was also enhanced ($R \approx 1.75$), whereas Y195F ($R = 0.5$) was reduced compared to the wild type (Figure 5). Step IIIp was not observed for either mutant (Figure 5). Further, the Y196H mutant was able to sequester iron as indicated by the presence of a weak LMCT band in the visible region of associated absorbance spectra, whereas Y195F did not develop a detectable LMCT band at the concentrations tested (data not shown).

DISCUSSION

Periplasmic binding proteins, including FbpA, capture their ligand via a Pac Man or Venus fly trap model (*39*). X-ray crystal structures of the apo and holo forms of FbpA show that the N-terminal and C-terminal domains close over the active site upon iron sequestration (*22*−*24*). The domains exhibit little change in secondary structure as a 21° hinge rotation occurs in the β-sheet section stretching between the two domains, pulling the protein from the open to the closed conformation. It is proposed that the C-terminal domain is preorganized for iron coordination through phosphate binding to the protein, and that Tyr195 and Tyr196 move little upon iron insertion (*22*−*24*). However, the rotamers of the N-terminal residues, His9 and Gly57, change conformation significantly when iron binds (*22*−*24*).

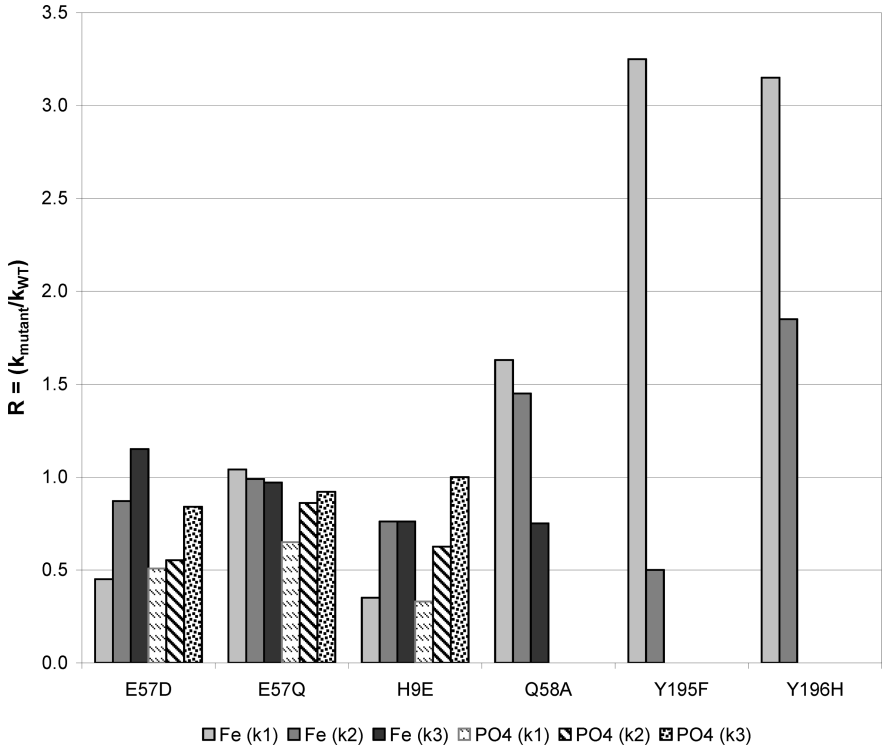

FIGURE 5: Average rate constant ratios (R = mutant/wild type). Rate constant ratios ($R = k_{mutant}/k_{wt}$) for pseudo-first-order rate constants for reaction 9 in the presence of excess phosphate or excess iron citrate. Conditions after mixing for a series of reactions where rate data were obtained over a range of phosphate concentrations [in the legend, $PO_4(k_n)$ (n = 1, 2, or 3)] represents k_{Ip}, k_{IIp}, and k_{IIIp}, respectively, in Scheme 4): 1, 2, 3, 5, 7, and 10 mM Na_2HPO_4; 0.007 mM apo-FbpA; 0.1 mM Fe(Cit)′; 0.05 M MES; 0.15 M $NaClO_4$; and pH 6.5. Conditions after mixing for a series of reactions where rate data were obtained over a range of Fe(Cit)′ concentrations [in the legend, Fe(k_n) (n = 1, 2, or 3) represents k_{Ip}, k_{IIp}, and k_{IIIp}, respectively in Scheme 4]: 0.1, 0.2, 0.3, 0.5, 0.7, and 1.0 mM Fe(Cit)′; 0.007 mM apo-FbpA; 5 mM Na_2HPO_4; 0.05 M MES; 0.15 M $NaClO_4$; and pH 6.5.

Via comparison with previous results obtained for delivery of Fe^{3+} to apo-FbpA from Fe(NTA) in the absence and presence of phosphate (*25*) and with data presented here, we suggest that the Fe^{3+} sequestration process is initiated through coordination at the N-terminal domain side chains. Further, we advocate that FbpA may also be considered as a transporter of FeX (X = coordinating synergistic anion) in addition to "naked" or free Fe^{3+} as previously suggested (*23*, *40*). A discussion of these assertions follows.

It is instructive to compare the results of the insertion of Fe(Cit)′ into apo-FbpA with the corresponding kinetics for Fe(NTA) insertion (*25*). In the absence of PO_4^{3-}, the insertion occurs in two distinguishable steps to produce FeFbpA-Cit and FeFbpA-NTA. An intermediate is formed [(FeX)FbpA-X*, where X is Cit to NTA] with an equilibrium constant of 10^4 M^{-1} in each case (Table 1). Although the initial step is zero-order in Fe(Cit)′, but first-order in Fe(NTA), at millimolar concentrations the rates are comparable, with a $t_{1/2}$ of 0.6−1.0 s for formation of the intermediate in each case under an identical set of arbitrary conditions (Table 1). The relaxation of the intermediate (FeX)FbpA-X* to FeFbpA-X (X is Cit or NTA) proceeds approximately 4 times faster in the NTA case with a rate constant 4.8×10^{-3} s^{-1} when X is Cit and 2.2×10^{-2} s^{-1} when X is NTA (Table 1). Although the rates of relaxation to FeFbpA-X are different, both Fe(Cit)′ and Fe(NTA) react via the same process through an (FeX)FbpA-X* intermediate assembly. The presence of phosphate in both Fe(Cit)′ and Fe(NTA) insertion reactions increases the number of kinetically observable steps from two to three to produce FeFbpA-Cit and FeFbpA-NTA, respectively (*25*).

Scheme 3 summarizes our kinetic data obtained using wild-type FbpA and inferences from our FbpA mutant studies for the stepwise process of insertion of iron into FbpA in the absence of phosphate. There is no apparent involvement of iron or citrate in the kinetics of step Ic. Consistent with this observation is the comparison of parameters for Fe(Cit)′ and Fe(NTA) in Tables 1 and 2 (row 2, columns 2 and 6), which show analogous first-step kinetics for these two complexes. Assuming the protein side chains are involved in the same sequence in the absence and presence of phosphate, initial sequestration of Fe^{3+} occurs at the N-terminal domain as indicated by the mutant studies. A 50% relative fluorescence amplitude change characteristic of iron tyrosine fluorescence quenching suggests the coordination of at least one tyrosine residue in the first step of the Fe^{3+} insertion process. This is confirmed by absorbance measurements consistent with Tyr−Fe LMCT band formation.

In step IIc of the Fe(Cit)′ system, the second tyrosine enters into the iron coordination shell (Scheme 3) as indicated by a second large fluorescence quenching amplitude change (50%) equal to that of the first step. In a comparison of the rate constants of the second steps, the transfer of iron from citrate is 5 times slower than from NTA under similar experimental conditions (Table 1). This may reflect differences in the lability of the first coordination shell in Fe(Cit)′ and Fe(NTA).

Scheme 4 represents an iron sequestration model for FbpA in the presence of phosphate and is based on our results for wild-type and mutant FbpA. Here FeX enters as a unit when introduced to apo-FbpA-PO_4. The pre-equilibrium reaction involving phosphate and FbpA results in the preorganization of the binding site tyrosines on the C-terminal domain (*24*, *41*). In the first step of the Fe−citrate−phosphate mechanism (Scheme 4), the lower level of fluorescence quenching (approximately 10%) suggests that the fluorescent side chains may be less accessible and indicates that Fe(Cit)′ is close but not bound as efficiently to the binding site tyrosines (Tyr195 and

Scheme 3: Iron Sequestration Model for the Apo-FbpA + Fe(Cit) Reaction[a]

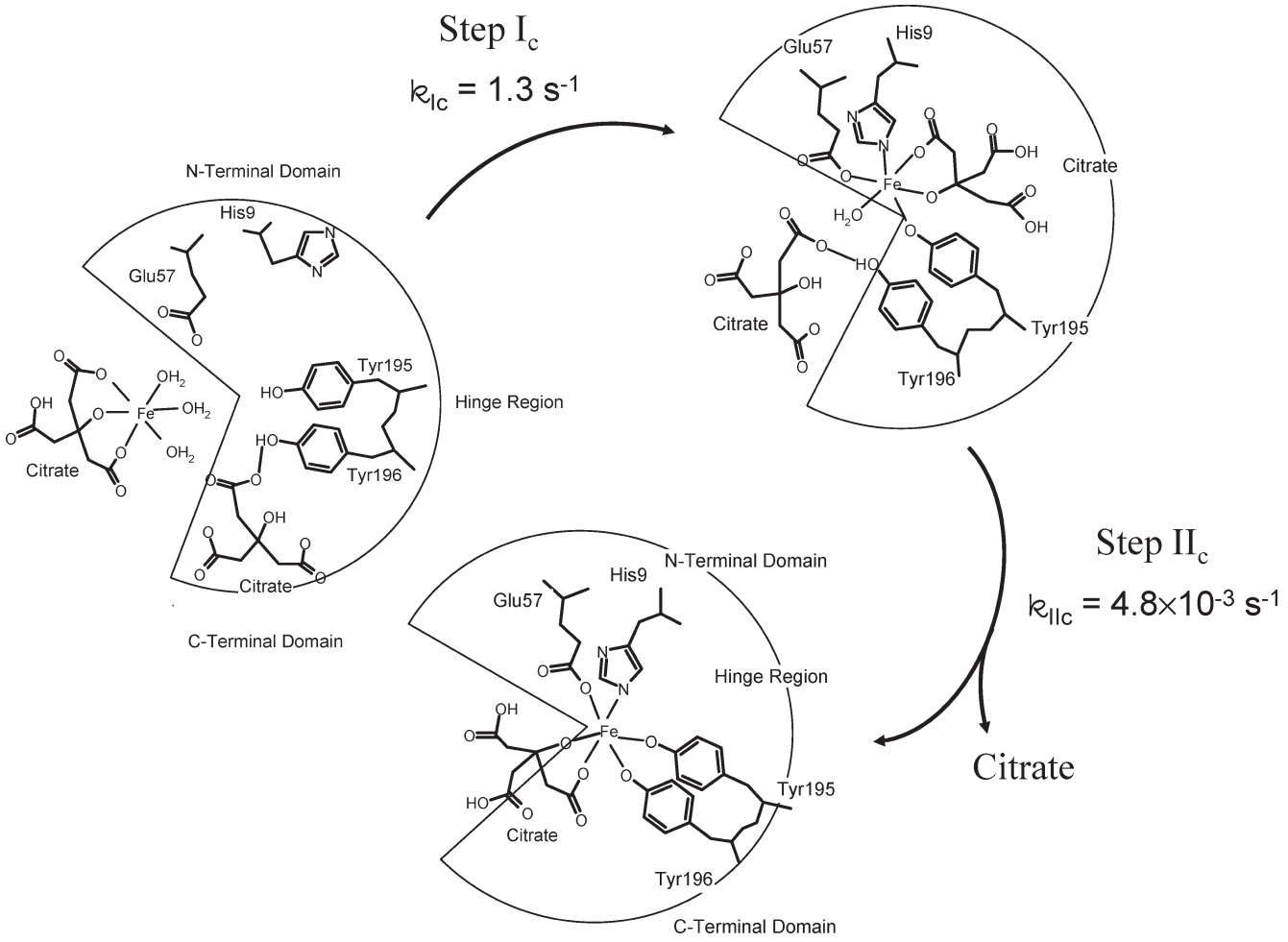

[a]Monocitrate iron species used in the illustration for the sake of clarity. Steps I and II exhibit equal fluorescence quenching amplitudes: 50% for step I and 50% for step II.

Tyr196). Interaction with the N-terminal residues is suggested by the N-terminal residue mutation results (Figure 5) in a mechanism similar to that observed in the first step of the Fe−NTA−phosphate system (*25*).

The second step of iron transfer is dependent upon phosphate concentration and likely reflects the equilibrium of eq 10 (Figure 4, inset), while the role of the iron chelator (citrate) is less obvious. Fluorescence is quenched by another 45% in step IIp which suggests iron coordination by one of the binding site tyrosines (Scheme 4). The final change in fluorescence intensity (approximately 45% quenching) in step IIIp indicates coordination by the second binding site tyrosine (Scheme 4).

Comparison of the wild-type kinetics to that of the binding mutants provides additional insight into the mechanism presented in Scheme 4. The loss of only one phenolate residue (Y195F) had a strong effect on iron sequestration, even though the in silico analysis of the replacement indicated molecular goodness of fit, leaving three properly aligned residues available for iron binding. Compared to the drastic effects of the single Tyr replacement with a nonbinding residue (Y195F), the Y196H mutant offered a binding site still outfitted with four functional groups capable of binding iron. Thus, the Y196H mutation made it possible to test C-terminal domain effects without losing iron coordination. Histidine is shorter than tyrosine, but this borderline hard/soft Lewis base is capable of coordinating Fe^{3+} and may even incorporate a bridging water molecule if present in the binding pocket, provided there is room.

For each of the Tyr mutants, only one Tyr residue remained to report iron interactions. Although the lack of a strong LMCT band is generally indicative of an inability to sequester iron, here the reduced absorptivity is proposed to reflect the fact that only one of the two tyrosines is available to report the presence of iron. If the iron binding pocket of the Tyr mutants is more accessible because of a lack of Tyr preorganization, the initial interaction of an approaching iron cation with the remaining Tyr could presumably result in more efficient quenching during step Ip. The reduced quenching amplitude of step IIp of Y195F and the loss of the kinetic mode fluorescence quenching in step IIIp for both protein mutants demonstrate a disruption in the ability to sequester iron and are strong indications of C-terminal domain effects later in the mechanism of the iron sequestration process. This is interesting in that although Y196H exhibits a weak LMCT band indicating Fe^{3+} coordination, Y196F does not exhibit a detectable LMCT band. The apparent loss of efficient iron sequestration for Y195F may be a result of the loss of phosphate−Fe^{3+}−Tyr195 interactions which are predicted to stabilize the closed form of the protein.

A final step (step IVp) occurs outside the time limits governing stopped-flow reactions reported here, but absorbance data clearly show anion exchange occurs in the final transition to the

Scheme 4: Iron Sequestration Model for the Apo-FbpA + Fe(Cit)(PO_4) Reaction[a]

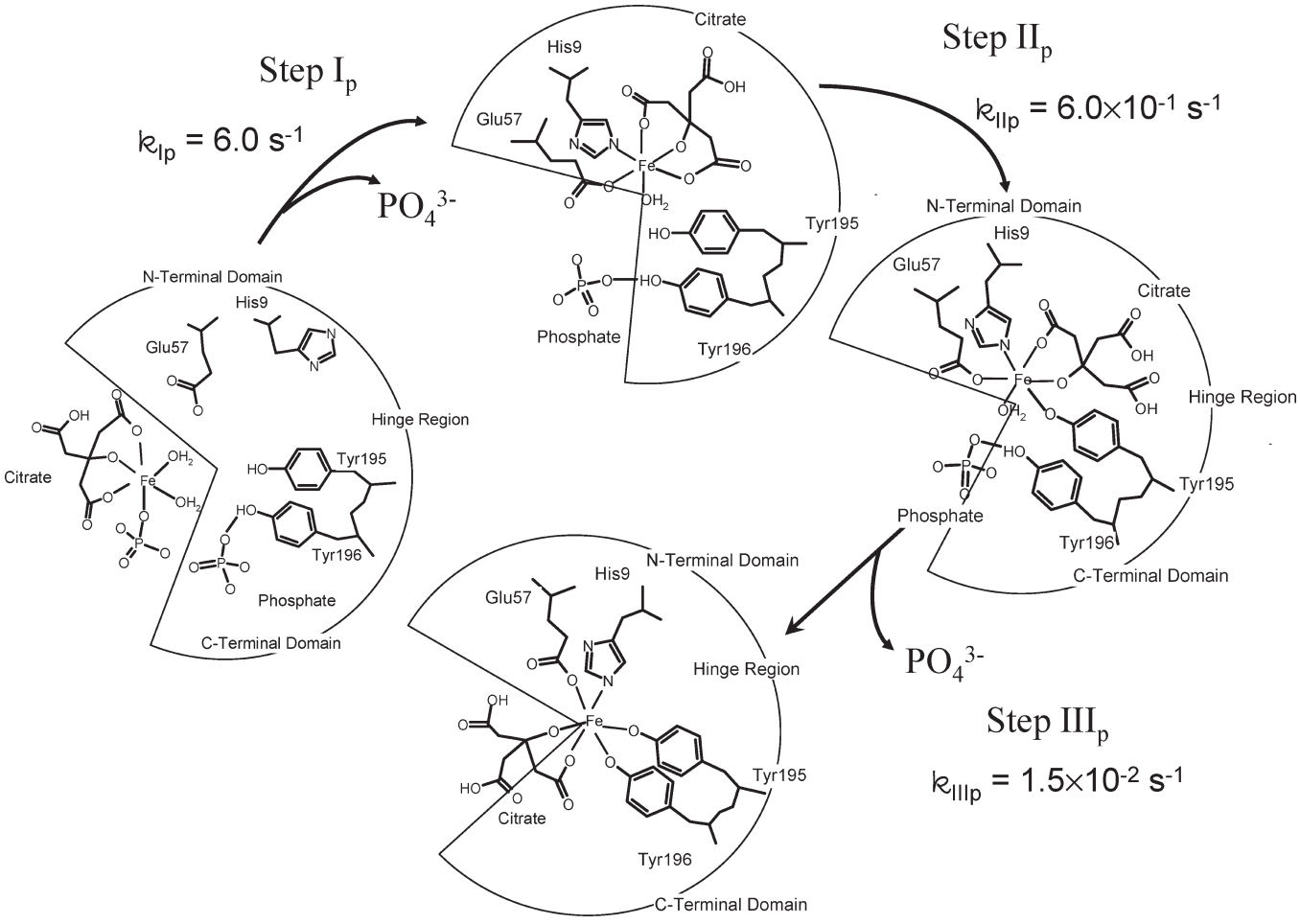

[a]Fluorescence quenching amplitudes: 10% for step I , 45% for step II, and 45% for step III.

phosphate form of the FeFbpA-PO_4 assembly, which is stable with respect to the loss of iron over the period of several days. A similar observation is made for the Fe(NTA) system, where FeFbpA-NTA is formed initially as the kinetic product, but eventually on a slower time scale, FeFbpA-PO_4 is formed as the thermodynamic product. A comparison of half-lives for this final anion exchange is as follows. For FeFbpA-Cit/PO_4, $t_{1/2}$ = 20 h [0.1 mM Fe(Cit)′, 5.0 mM $H_xPO_4^{y-}$, 50 μM FbpA, 50 mM MES, 150 mM $NaClO_4$, pH 6.5, and 25 °C], and for FeFbpA-NTA/PO_4, $t_{1/2}$ = 2 h [0.1 mM Fe(NTA), 1.0 mM $H_xPO_4^{y-}$, 50 μM FbpA, 50 mM MES, 150 mM $NaClO_4$, pH 6.5, and 25 °C] (*25*). In each case, the kinetically controlled product in the presence of excess phosphate is FeFbpA-X (X is Cit or NTA) (eq 15), which eventually exchanges to the thermodynamically controlled product FeFbpA-PO_4 (eq 16). The fact that the anion exchange requires a much longer time in the citrate system most likely reflects the fact that apo-FbpA has a 50-fold higher affinity for citrate than for NTA (*19*).

$$\text{FeX} + \text{apo-FbpA-PO}_4 \leftrightarrows \text{FeFbpA-X} + \text{PO}_4 \quad \text{kinetic product} \tag{15}$$

$$\text{FeFbpA-X} + \text{PO}_4 \leftrightarrows \text{FeFbpA-PO}_4 + \text{X} \quad \text{thermodynamic product} \tag{16}$$

These data illustrate the fact that for the small molecule iron carriers citrate and NTA, FeX reacts with apo-FbpA-PO_4 to form FeFbpA-X as the kinetically controlled product (eq 15), with eventual anion exchange in the presence of excess phosphate to FeFbpA-PO_4 (eq 16). This further suggests that FbpA should be considered an FeX carrier when being loaded via a small molecule source, rather than just a naked Fe^{3+} carrier. This concept was first introduced by Shouldice et al. in a structural paper showing FeEDTA bound to a mutant of FbpA (*42*). This shows that FbpA can accommodate an iron/anion−ligand complex by adopting an open conformation, in the case of Shouldice et al. with Fe-EDTA bound to form an Fe-EDTA-FbpA assembly (*42*, *43*). In this model, FbpA may be more like a siderophore periplasmic binding protein (e.g., FepB) (*44*) which transports iron coordinated to a siderophore through the periplasm of *E. coli*; in the case of FbpA, the anion (e.g., citrate or NTA) takes the place of the siderophore carrier. That FbpA can incorporate different anions suggests that sequestration of FeX involves an adaptive protein−protein interface suited to binding alternative anions for the achievement of an iron-bound form of FbpA.

An overall objective of our work is to understand the in vivo mechanisms of iron citrate and iron phosphate uptake in *Neisseria* in order to understand the role and significance of these processes in pathogenesis. The ability of *Neisseria* to use ferric citrate as an iron source and the ease of exchange of iron between citrate and FbpA may aggravate the outcome of infections and impose an increased risk in host cells with compromised iron withholding defenses (*9*, *12*). Generalized iron overload associated with non-transferrin-bound iron in dialysis patients and under conditions such as hemochromatosis and thalassaemia is known to result

in an increased risk of infection by microorganisms which utilize low-molecular mass iron complexes, including complexes with citrate (*45*). Whether sequestration of iron from ferric citrate by FbpA plays an important role in gonococcal and meningococcal infections remains to be further examined. However, the fact that citrate is available to *Neisseria* and can be used for iron exchange with FbpA clearly suggests such a role.

ACKNOWLEDGMENT

We acknowledge Drs. David C. and Jane S. Richardson (Duke University) for their assistance and guidance during the depiction and in silico analysis of the iron binding mutants of FbpA used in this study.

SUPPORTING INFORMATION AVAILABLE

Additional kinetic plots, in silico models of FbpA mutants, and MALDI-TOF and CD characterization of point mutations. This material is available free of charge via the Internet at http://pubs.acs.org.

REFERENCES

1. Clarke, T. E., Tari, L. W., and Vogel, H. J. (2001) Structural biology of bacterial iron uptake systems. *Curr. Top. Med. Chem. 1*, 7–30.
2. Mietzner, T. A., and Morse, S. A. (1994) The role of iron-binding proteins in the survival of pathogenic bacteria. *Annu. Rev. Nutr. 14*, 471–493.
3. Gray-Owen, S. D., and Schryvers, A. B. (1996) Bacterial transferrin and lactoferrin receptors. *Trends Microbiol. 4*, 185–191.
4. Mietzner, T. A., Bolan, G., Schoolnik, G. K., and Morse, S. A. (1987) Purification and characterization of the major iron-regulated protein expressed by pathogenic Neisseriae. *J. Exp. Med. 165*, 1041–1057.
5. Adhikari, P., Berish, S. A., Nowalk, A. J., Veraldi, K. L., Morse, S. A., and Mietzner, T. A. (1996) The fbpABC locus of *Neisseria gonorrhoeae* functions in the periplasm-to-cytosol transport of iron. *J. Bacteriol. 178*, 2145–2149.
6. Ferguson, S. J. (1992) The Periplasm. In Prokaryotic Structure and Function: A New Perspective (Mohan, S., Dow, C., and Cole, J. A., Eds.) pp 311−339, Cambridge University Press, New York.
7. Payne, S. M., and Finkelstein, R. A. (1975) Pathogenesis and immunology of experimental gonococcal infection: Role of iron in virulence. *Infect. Immun. 12*, 1313–1318.
8. Brener, D., DeVoe, I. W., and Holbein, B. E. (1981) Increased virulence of *Neisseria meningitidis* after in vitro iron-limited growth at low pH. *Infect. Immun. 33*, 59–66.
9. van Putten, J. P. M. (1990) Iron acquisition and the pathogenesis of meningococcal and gonococcal disease. *Med. Microbiol. Immunol. 179*, 289–295.
10. Petrat, F., Rauen, U., and De Groot, H. (1999) Determination of the chelatable iron pool of isolated rat hepatocytes by digital fluorescence microscopy using the fluorescent probe, phen green SK. *Hepatology 29*, 1171–1179.
11. Budzikiewicz, H. (2005) Bacterial citrate siderophores. *Mini-Rev. Org. Chem. 2*, 119–124.
12. Archibald, F. S., and DeVoe, I. W. (1980) Iron acquisition by *Neisseria meningitidis* in vitro. *Infect. Immun. 27*, 322–334.
13. Simonson, C., Trivett, T., and DeVoe, I. W. (1981) Energy-independent uptake of iron from citrate by isolated outer membranes of *Neisseria meningitidis*. *Infect. Immun. 31*, 547–553.
14. Politi, L., Chiaraluce, R., Consalvi, V., Cerulli, N., and Scandurra, R. (1989) Oxalate, phosphate and sulphate determination in serum and urine by ion chromatography. *Clin. Chim. Acta 184*, 155–166.
15. Lentner, C. (1984) Geigy Scientific Tables, vol 3, Physical Chemistry Composition of Blood Hematology Somatometric Data, pp 79, 109, Ciba-Geigy Corp., West Caldwell, NJ.
16. Taboy, C. H., Vaughan, K. G., Mietzner, T. A., Aisen, P., and Crumbliss, A. L. (2001) Fe^{3+} coordination and redox properties of a bacterial transferrin. *J. Biol. Chem. 276*, 2719–2724.
17. Boukhalfa, H., Anderson, D. S., Mietzner, T. A., and Crumbliss, A. L. (2003) Kinetics and mechanism of iron release from the bacterial ferric binding protein nFbp: Exogenous anion influence and comparison with mammalian transferrin. *J. Biol. Inorg. Chem. 8*, 881–892.
18. Dhungana, S., Taboy, C. H., Anderson, D. S., Vaughan, K. G., Aisen, P., Mietzner, T. A., and Crumbliss, A. L. (2003) The influence of the synergistic anion on iron chelation by ferric binding protein, a bacterial transferrin. *Proc. Natl. Acad. Sci. U.S.A. 100*, 3659–3664.
19. Heymann, J. J., Weaver, K. D., Mietzner, T. A., and Crumbliss, A. L. (2007) Sulfate as a synergistic anion facilitating iron binding by the bacterial transferrin FbpA: The origins and effects of anion promiscuity. *J. Am. Chem. Soc. 129*, 9704–9712.
20. Heymann, J. J., Gabričević, M., Mietzner, T. A., and Crumbliss, A. L. (2010) Kinetics and mechanism of exogenous anion exchange in FeFbpA-NTA: Significance of periplasmic anion lability and anion binding activity of ferric binding protein A. *J. Biol. Inorg. Chem. 15*, 237–248.
21. Guo, M., Harvey, I., Yang, W., Coghill, L., Campopiano, D. J., Parkinson, J. A., MacGillivray, R. T. A., Harris, W. R., and Sadler, P. J. (2003) Synergistic anion and metal binding to the ferric ion-binding protein from *Neisseria gonorrhoeae*. *J. Biol. Chem. 278*, 2490–2502.
22. McRee, D. E., Bruns, C. M., Williams, P. A., Mietzner, T. A., Nunn, R. (1999) *Neisseria gonorrhoeae* ferric binding protein, RSCB PDB 1D9Y.
23. Bruns, C. M., Nowalk, A. J., Arvai, A. S., McTigue, M. A., Vaughan, K. G., Mietzner, T. A., and McRee, D. E. (1997) Structure of *Haemophilus influenzae* Fe^{3+}-binding protein reveals convergent evolution within a superfamily. *Nat. Struct. Biol. 4*, 919–924.
24. Bruns, C. M., Anderson, D. S., Vaughan, K. G., Williams, P. A., Nowalk, A. J., McRee, D. E., and Mietzner, T. A. (2001) Crystallographic and biochemical analyses of the metal-free *Haemophilus influenzae* Fe^{3+}-binding protein. *Biochemistry 40*, 15631–15637.
25. Gabričević, M., Anderson, D. S., Mietzner, T. A., and Crumbliss, A. L. (2004) Kinetics and mechanism of iron(III) complexation by ferric binding protein: The role of phosphate. *Biochemistry 43*, 5811–5819.
26. Bastian, R., Weberling, R., and Palilla, F. (1956) Determination of iron by ultraviolet spectrophotometry. *Anal. Chem. 28*, 459–462.
27. Spiro, T. G., Bates, G. W., and Saltman, P. (1967) The hydrolytic polymerization of ferric citrate. II. The influence of excess citrate. *J. Am. Chem. Soc. 89*, 5559–5562.
28. Berish, S. A., Mietzner, T. A., Mayer, L. W., Genco, C. A., Holloway, B. P., and Morse, S. A. (1990) Molecular cloning and characterization of the structural gene for the major iron-regulated protein expressed by *Neisseria gonorrhoeae*. *J. Exp. Med. 171*, 1535–1546.
29. Königsberger, L.-C., Königsberger, E., May, P. M., and Hefter, G. T. (2000) Complexation of iron(III) and iron(II) by citrate. Implications for iron speciation in blood plasma. *J. Inorg. Biochem. 78*, 175–184.
30. Motekaitis, R. J. (2001) in The National Institute of Standards and Technology (NIST) Standard Reference Database 46, The National Institute of Standards and Technology, Gaithersburg, MD.
31. Silva, A. M. N., Kong, X.-L., Parkin, M. C., Cammack, R., and Hider, R. C. (2009) Iron(III) citrate speciation in aqueous solution. *Dalton Trans.,* 8616–8625.
32. Ramamoorthy, S., and Manning, P. G. (1974) Formation and stabilities of quaternary complexes of Fe^{3+} in solutions of phosphate, fulvate and simple carboxylate ligands. *Inorg. Nucl. Chem. Lett. 10*, 109–114.
33. Tonomura, B., Nakatani, H., Ohnishi, M., Yamaguchi-Ito, J., and Hiromi, K. (1978) Test reactions for a stopped-flow apparatus: Reduction of 2,6-dichlorophenolindophenol and potassium ferricyanide by L-ascorbic acid. *Anal. Biochem. 84*, 370–383.
34. Bates, G. W., Billups, C., and Saltman, P. (1967) The kinetics and mechanism of iron(III) exchange between chelates and transferrin. I. The complexes of citrate and nitrilotriacetic acid. *J. Biol. Chem. 242*, 2810–2815.
35. Cabell, L. A., Best, M. D., Lavigne, J. J., Schneider, S. E., Perreault, D. M., Monahan, M.-K., and Anslyn, E. V. (2001) Metal triggered fluorescence sensing of citrate using a synthetic receptor. *J. Chem. Soc., Perkin Trans. 2*, 315–323.
36. De Santis, G., Fabbrizzi, L., Licchelli, M., Poggi, A., and Taglietti, A. (1996) Molecular recognition of carboxylate ions based on the metal-ligand interaction and signaled through fluorescence quenching. *Angew. Chem., Int. Ed. 35*, 202–204.
37. Pakdaman, R., Petitjean, M., and El Hage Chahine, J.-M. (1998) Transferrins: A mechanism for iron uptake by lactoferrin. *Eur. J. Biochem. 254*, 144–153.
38. Bou Abdallah, F., and El Hage Chahine, J.-M. (1998) Transferrins. Hen ovo-transferrin, interaction with bicarbonate and iron uptake. *Eur. J. Biochem. 258*, 1022–1031.
39. Mao, B., Pear, M. R., McCammon, J. A., and Quiocho, F. A. (1982) Hinge-bending in L-arabinose-binding protein. The Venus's-flytrap model. *J. Biol. Chem. 257*, 1131–1133.
40. Crichton, R. R. (2009) Iron Metabolism: From Molecular Mechanisms to Clinical Consequences, 3rd ed., John Wiley & Sons, New York.

41. Zhu, H., Alexeev, D., Hunter, D. J. B., Campopiano, D. J., and Sadler, P. J. (2003) Oxo-iron clusters in a bacterial iron-trafficking protein: New roles for a conserved motif. *Biochem. J. 376*, 35–41.
42. Shouldice, S. R., Dougan, D. R., Skene, R. J., Tari, L. W., McRee, D. E., Yu, R.-H., and Schryvers, A. B. (2003) High resolution structure of an alternate form of the ferric ion binding protein from *Haemophilus influenzae*. *J. Biol. Chem. 278*, 11513–11519.
43. Weaver, K. D., and Crumbliss, A. L. (2003) Condensation: Commentary on high-resolution structure of an alternate form of the ferric ion binding protein from *Haemophilus influenzae*. *Chemtracts: Inorg. Chem. 16*, 715–721.
44. Pierce, J. R., and Earhart, C. F. (1986) *Escherichia coli* K-12 envelope proteins specifically required for ferrienterobactin uptake. *J. Bacteriol. 166*, 930–936.
45. Grootveld, M., Bell, J. D., Halliwell, B., Aruoma, O. I., Bomford, A., and Sadler, P. J. (1989) Non-transferrin-bound iron in plasma or serum from patients with idiopathic hemochromatosis. Characterization by high performance liquid chromatography and nuclear magnetic resonance spectroscopy. *J. Biol. Chem. 264*, 4417–4422.